S1 Detailed description of batch sorption experiments

For each region, a stock of freeze-dried active layer material was created by homogenizing multiple active layer samples from the respective region. An organic-rich leachate was generated by mixing 270 g of active layer material with 2700 mL of 18.2 MΩ (MilliQ) water (1:10 w/v) for 72 h on a shaker table rotating at 60 rpm. Dark conditions were maintained to prevent compositional shifts in DOM due to photodegradation (Mopper and Kieber, 2000). Leachates were extracted at 10 °C to mimic stream conditions in the Peel Plateau (Littlefair and Tank, 2018; Zolkos et al., 2022) and to reduce potential microbial activity. Active layer leachate was filtered to 0.2 µm by serial filtration through a precombusted (500 °C for 5 h) glass microfiber filter (1.2 µm pore size; Whatman GF/C), a sterile 0.45 µm polyethersulfone (PES) membrane filter (Sterlitech), and a sterile 0.22 µm PES membrane filter (Sterlitech). The leachate was adjusted to a pH of 6.5 (trace metal grade HCl) and to a conductivity of 135 µS cm (NaCl) to mimic stream conditions in the Peel Plateau (Kokelj et al., 2013; Malone et al., 2013; Zolkos et al., 2019). Filtered leachate was diluted with MilliQ water of the same pH and conductivity to create a series of five stock solutions of varying DOC concentrations. Aliquots for the measurement of DOC concentration, DOM composition, pH, and conductivity were reserved for each of the five stock solutions.

In 125 mL glass bottles, 5 g of sediment was combined with 100 mL of one of the five stock solutions (1:20 w/v). This was repeated for all five stock solutions in duplicate, totalling 10 bottles per sample. Samples were mixed for 48 h in the dark at 10 °C on a shaker table at 60 rpm following Kaiser et al. (1996). One bottle each containing the highest and lowest concentration stock solutions were incubated without sediment to control for DOM composition changes due to non-sorption effects (e.g., flocculation, photodegradation). Bottles were filtered using precombusted glass microfibre filter (1.2 µm pore size; Whatman GF/C) followed by a sterile 0.45 µm PES membrane filter (Sterlitech) and subsampled for dissolved organic carbon (DOC) concentration, dissolved organic matter (DOM) composition, pH, and conductivity. Analytes were analyzed as described in the main text.

S2 Detailed description of bio-incubation experiment

Bio-incubation treatments were prepared by leaching freeze-dried active layer sediment from the Peel Plateau (1:10 w/v), and filtering, as described above. The active layer leachate was divided into four 2 L bottles. In three of the bottles, 75 g of freeze-dried sediment (unmodified till, Holocene-modified till, and thawed debris from site SE in the Peel Plateau) was combined with 1500 mL of active layer leachate (1:20 w/v). Bottles were mixed for 48 h in the dark at 10 °C on a shaker table rotating at 60 rpm. Solutions were filtered to 0.22 µm, as described above and stored in the fridge at 4 °C overnight before the start of the bio-incubation the following day.

To create the microbial inoculum, approximately 6000 mL of water was collected from the Mackenzie River 2 km upstream from the town of Inuvik (68.33833, -133.70583) and immediately shipped in coolers to Edmonton. The following day, the river water was filtered to 1.2 µm with a precombusted glass microfiber filter (Whatman GF/C), to enable passage of microbes, but excluded microbial grazers from our experiments.

For each of the four treatment solutions, 630 mL of filtrate was inoculated with 70 mL of filtered river water (10% v/v inoculation). Flasks were aerated for 5 minutes with compressed air and allowed to rest for 10 minutes to degas to standardize the initial oxygen content. Triplicate glass bottles equipped with oxygen spot sensors (SP-PSt3-PSUP-YOPD5, PreSens GmbH) and one glass bottle for water chemistry analysis (see below) were then filled with 120 mL of aerated, inoculated solutions. Bottles were filled from the bottom up to prevent air bubbles.

Bottles for measurement of O_2 were capped with chlorobutyl isoprene stoppers and an aluminum crimp top to create a sealed bottle and to prevent oxygen exchange with the atmosphere and measured for initial oxygen content before placement in a dark incubator at 20 °C. Using the water chemistry bottle, dissolved inorganic carbon (DIC) measurements were taken promptly following experimental setup, and aliquots were collected for total dissolved nitrogen, total dissolved phosphorous, nitrite/nitrate, soluble reactive phosphorous, DOC, absorbance/fluorescence, pH, and conductivity. Oxygen measurements were taken every 24 h following experimental setup with a fibre-optic oxygen meter (Fibox 3; PreSens GmbH) until the end of the 14-day bio-incubation or until the bottle was terminated due to hypoxic conditions (< 2 mg L^{-1}).

At the end of the 14-day bio-incubation or when bottles reached hypoxic conditions, DIC was measured in each bottle, and the remaining water was refiltered through 0.45 µm PES filter. No flocs were observed on the filters. The filtrate was divided for DOC concentration, DOM composition, and pH measurements. DOC concentration, DOM composition, and DIC concentration were analyzed as detailed in the main text. Aliquots for nutrients were analyzed by flow injection analysis (Lachat QuikChem 8500 FIA automated ion analyzer) at the Biogeochemical Analytical Service Laboratory (BASL) at the University of Alberta.

S3 Detailed description of statistical analysis

Statistical analyses were performed in R (4.4.1; R Core Team, 2024) unless otherwise noted, using *tidyverse*, *dplyr,* and *ggplot2* for data management and visualization (Wickham, 2016; Wickham et al., 2019, 2023). Sediment biogeochemistry was explored with box and whisker plots, a principal component analysis, and one-way analysis of variance (ANOVA) tests, followed by Tukey Honestly Significant Difference (HSD) test when main effects were significant ($p < 0.05$) (see main text). To test for the effects of changing pH and conductivity on DOC concentration and DOM composition, paired t-tests were used to compare the pH and conductivity of the solution before and after exposure to sediment in the batch sorption experiment. Simple linear regressions were used to analyze relationships between sediment characteristics and sorption properties. A PCA was created with the PARAFAC components and absorbance indices to visualize shifts in DOM composition of stock solutions following exposure to permafrost sediments in the batch sorption and bio-incubation experiments. Scores of Principal Component 1 and 2 were extracted to summarize DOM composition for later analyses. To confirm heterotrophic respiration as the driver of DOM biodegradation in the bio-incubation experiment, gain in DIC and loss of dissolved O_2 were normalized to initial TOC concentrations and visualized with a biplot. To compare carbon mineralization between treatments in the bio-incubation experiment, the rate of oxygen loss was calculated using the first-order decay and visualized with a point

plot. Drivers of oxygen loss rates were explored through similar linear regressions. All summary statistics are reported as mean ± standard error, unless otherwise noted.

Table S1. Sampling locations of different sediment types in northwestern Canada. Sites with different identifiers in previous studies are noted in brackets under Site Code. Coordinates are reported in decimal degrees. Multiple samples collected from the same sediment type at one site are indicated in brackets, with depths of each sample listed from shallow to deep. Sediment types represented in the batch sorption and incubation experiments are italicized and denoted with a *, respectively.

Region	Site Code	Landform	Latitude	Longitude	Elevation (m ASL)	Sediment Type	Depth Below Surface (m)
Peel Plateau	CRB	Retrogressive Thaw Slump	67.18309	-135.73224	598	Active Layer	<0.5
						Holocene-Modified Till (*n* = 3)	>5 (all)
						Colluvium (*n* = 3)	2.5, 4, 4
						Unmodified Till (*n* = 3)	2, 2, 3
						Thawed Debris (*n* = 2)	<0.5 (all)
	CRB23 (SD)	Retrogressive Thaw Slump	67.18117	-135.72617	586	*Holocene-Modified Till*	2
						Colluvium	<1
						Unmodified Till	3.5
						Thawed Debris (*n* = 2)	<0.5 (all)
	CRB5	Retrogressive Thaw Slump	67.18107	-135.73892	625	Active Layer	<0.5
						Holocene-Modified Till	1
						Unmodified Till	2
						Thawed Debris (*n* = 2)	<0.5 (all)
	E5	Retrogressive Thaw Slump	68.19404	-135.48799	113	Thawed Debris (*n* = 2)	<0.5 (all)
	WR1 (E1)	Retrogressive Thaw Slump	68.11418	-135.67833	310	*Holocene-Modified Till* (*n* = 3)	15, 16, 17
						Unmodified Till (*n* = 3)	>15 (all)
						Thawed Debris (*n* = 2)	<0.5 (all)
	FM2	Retrogressive Thaw Slump	67.25559	-135.22255	248	*Unmodified Till*	2.5
						Thawed Debris (*n* = 2)	<0.5 (all)
	FM3	Retrogressive Thaw Slump	67.25595	-135.27710	375	Unmodified Till	1.5
						Thawed Debris (*n* = 2)	<0.5 (all)
	HB	Retrogressive Thaw Slump	67.238611	-135.82400	650	Active Layer	<0.5
	HF	Retrogressive Thaw Slump	67.3251	-135.90300	641	Active Layer	<0.5
	HL		67.52112	-135.29446	260	*Colluvium* (*n* = 3)	1, 1.5, 2

		Retrogressive Thaw Slump				*Unmodified Till* (*n* = 3)	4, 5, 6
						Thawed Debris (*n* = 2)	<0.5 (all)
	SE	Retrogressive Thaw Slump	67.14662	-135.71726	553	**Holocene-Modified Till* (*n* = 3)	>10 (all)
						**Unmodified Till* (*n* = 3)	>10 (all)
						**Thawed Debris* (*n* = 5)	<0.5 (all)
Central Mackenzie Valley	KRT	Landslide	64.28861	-125.85700	450	Active Layer	<0.5
						Colluvium (*n* = 2)	>18, >18
						Thawed Debris	<0.5
	KRTC	Landslide	63.93705	-125.84944	531	*Colluvium* (*n* = 3)	3, 3.5, 4.5
						Thawed Debris (*n* = 2)	<0.5 (all)
	RRT3	Landslide	64.03266	-125.56167	532	*Glaciolacustrine* (*n* = 3)	3, 3.5, 4
						Thawed Debris (*n* = 3)	<0.5 (all)
Klondike	MG	Mining Excavation Site	63.93776	-138.88974	556	*Yedoma* (*n* = 4)	3, 3.5, 6, 7
	LB	Mining Excavation Site	63.81195	-139.06968	540	*Yedoma* (*n* = 3)	6, 6.5, 7
	W1	Undisturbed Forest	63.80551	-138.60818	644	Active Layer	<1
	BW1	Burned Forest	63.80475	-138.60425	643	Active Layer	<1
	RD[2]2	Disturbed (Road) Forest	63.80373	-138.60955	631	Active Layer	<1

Table S2. Detection limits for parameters assessed to describe sediment characteristics and nutrient concentrations.

Parameter	Instrument	Detection Limit	Laboratory
Grain Size	Mastersizer 3000 (D422-ASTM, Malvern)	10 nm	Permafrost ArChives Laboratory (University of Alberta)
Elemental C	Vario ISOTOPE Cube (Elementar)	0.01 %	Ján Veizer Stable Isotope Laboratory (University of Ottawa)
Elemental N	Vario ISOTOPE Cube (Elementar)	0.01 %	Ján Veizer Stable Isotope Laboratory (University of Ottawa)
pH	Benchtop pH probe (Mettler Toledo)	N/A	University of Alberta
Conductivity	YSI multiparameter probe (YSI Professional Plus)	0.1 µS cm^{-1}	University of Alberta
Al	ICP-OES (Thermo Scientific ICAP6300)	3.6 µg L^{-1}	BASL (University of Alberta)
Ca	ICP-OES (Thermo Scientific ICAP6300)	0.01 mg L^{-1}	BASL (University of Alberta)
Fe	ICP-OES (Thermo Scientific ICAP6300)	0.02 µg L^{-1}	BASL (University of Alberta)
Mn	ICP-OES (Thermo Scientific ICAP6300)	14.5 µg L^{-1}	BASL (University of Alberta)
Mineral Presence	Ultima IV x-ray diffractometer	1-5 %	X-Ray Diffraction Laboratory (University of Alberta)
Dissolved Organic Carbon (DOC)	Shimadzu TOC-5000A	4 µg L^{-1}	University of Alberta
Total Dissolved Phosphorous (TDP)	Lachat QuikChem 8500 FIA automated ion analyzer	1 µg L^{-1}	BASL (University of Alberta)
Soluble Reactive Phosphorous (SRP)	Lachat QuikChem 8500 FIA automated ion analyzer	1 µg L^{-1}	BASL (University of Alberta)
NO_2NO_3	Lachat QuikChem 8500 FIA automated ion analyzer	2 µg L^{-1}	BASL (University of Alberta)
Total Dissolved Nitrogen (TDN)	Lachat QuikChem 8500 FIA automated ion analyzer	11 µg L^{-1}	BASL (University of Alberta)
Dissolved Inorganic Carbon (DIC)	AS-C3 DIC Analyzer (Apollo SciTech)	0.2 mM L^{-1}	University of Alberta

Note. BASL, Biogeochemical Analytical Service Laboratory.

Table S3. Parameters of the initial mass isotherms of the sorption of dissolved organic matter to thawed permafrost sediments.

Sample ID	*m*	*b* (mg L^{-1})	R^2
PP_CRB_UT2	0.36	3.2	0.84
PP_CRB_HT3	0.37	3.9	0.77
PP_CRB_TD	0.38	6.7	0.83
PP_CRB_CO2	0.18	3.9	0.59
PP_CRB23_UT	-0.02	6.0	0.06
PP_CRB23_HT	0.39	6.4	0.87
PP_CRB23_TD	0.45	6.0	0.90
PP_CRB23_CO	0.27	4.4	0.94
PP_SE_HT1	0.28	2.9	0.96
PP_SE_UT3	0.39	8.1	0.72
PP_SE_TD4	0.27	3.8	0.93
PP_SE_TD	0.18	1.4	0.80
PP_HL_UT	0.30	2.3	0.98
PP_HL_CO2	0.34	2.1	0.99
PP_FM2_UT	0.26	2.2	0.95
PP_FM2_TD	0.38	0.8	0.98
PP_FM2_TD2	0.33	1.0	0.98
PP_WR1_HT3	0.27	8.0	0.76
PP_WR1_UT2	0.17	3.7	0.65
PP_WR1_TD	0.33	2.2	0.95
CMV_KRT_CO2	0.16	4.3	0.84
CMV_KRT_CO1	0.26	1.2	0.92
CMV_KRTC_TD	0.15	2.3	0.93
CMV_KRTC_CO3	0.17	1.3	0.76
CMV_KRTC_CO1	0.30	0.3	0.97
CMV_RRT3_GL2	0.28	4.7	0.96
CMV_RRT3_GL1	0.23	2.3	0.98
CMV_RRT3_TD1	0.22	0.8	0.97
KL_LB_YE3	0.16	46.1	0.60
KL_LB_YE1	0.22	57.4	0.62
KL_MG_YE4	0.13	8.2	0.87
KL_MG_YE1	0.18	28.5	0.78

Table S4. Spectral properties (maximum excitation (Ex) and emission (Em) wavelengths) of the six components identified with PARAFAC analysis, their associated dissolved organic matter characteristics, and reference to PARAFAC components previously identified in other studies via comparison with the OpenFluor database. Bracketed excitation and emission wavelengths show secondary peaks, where applicable. Corresponding components found in references are in brackets under the References column.

Component	Maximum Wavelength		General Description	Potential Molecular Characteristics	References
	Ex (nm)	*Em (nm)*			
C1	245 (340)	446.65	Terrestrial Humic-like	Highly aromatic	Orlova et al. (2024) (C1) Kothawala et al. (2014) (C4)
C2	245 (400)	504.47	Terrestrial Humic-like	Reduced quinone-like (derivatives of aromatic compounds)	(C3) Cory and McKnight (2005) (HQ)
C3	245 (320)	386.64	Terrestrial Humic-like Intermediate compounds in degradation process	Low aromatic content	Orlova et al. (2024) (C3) Chen et al. (2021) (C1) Coble (1996) (A, C)
C4	255	432.76	Terrestrial Humic-like Intermediate compounds in degradation process	Moderate aromatic content	Osburn et al. (2017) (C3) DeFrancesco and Guéguen (2021) (C4) Coble (1996) (A)
C5	305 (245)	418.9	Microbially-produced Humic-like	Aliphatic Low molecular weight	Podgorski et al. (2018) (C4) Lambert et al. (2016) (C2) Coble (1996) (M)
C6	270	302.18	Microbially-produced Protein-like	Tyrosine-like Low molecular weight	Dainard et al. (2015) (C4) Walker et al. (2009) (C5) Coble (1996) (B)

Table S5. Nutrient concentrations and biogeochemical properties of permafrost sediment-exposed stock solutions inoculated with river water (10 % v/v) prior to the bio-incubation.

Stock Solution	TDP ($\mu g\ L^{-1}$)	SRP ($\mu g\ L^{-1}$)	TDN ($\mu g\ L^{-1}$)	NH_4 ($\mu g\ L^{-1}$)	NO_2NO_3 ($\mu g\ L^{-1}$)	DOC ($mg\ L^{-1}$)	pH	Conductivity ($\mu S\ cm^{-1}$)	DIC ($\mu M\ L^{-1}$)
Inoculated MilliQ	8	9	40	2.8	4	1.6	6.5	21.3	160
Active Layer Stock Solution	38	4	411	20.9	3	13.6	6.8	40.2	163
Unmodified Till	41	5	1640	1090	15	18.0	7.4	187.3	630
Holocene-Modified Till	38	6	943	506	15	11.9	7.2	113.6	501
Thawed Debris	37	5	567	120	34	13.0	7.1	232.8	320

Note. TDP, total dissolved phosphorous; SRP, soluble reactive phosphorous; TDN, total dissolved nitrogen; DOC, dissolved organic carbon; DIC, dissolved inorganic carbon.

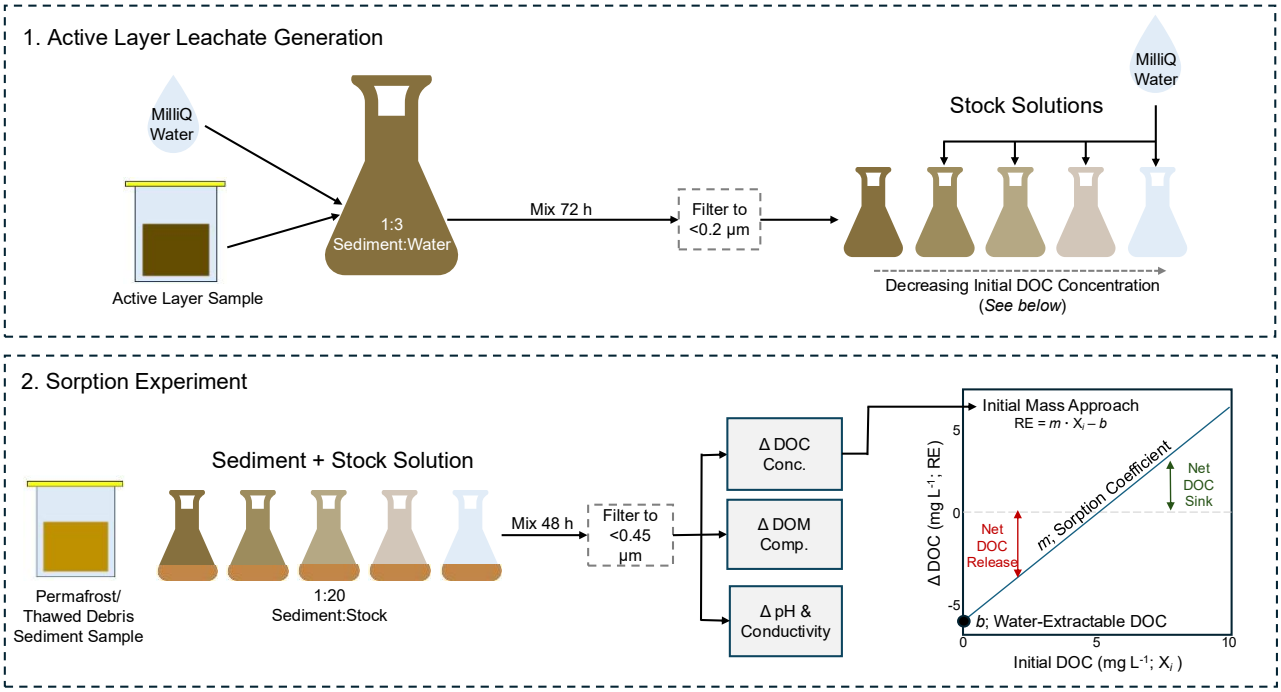

Figure S1. Schematic diagram illustrating the batch sorption experiment.

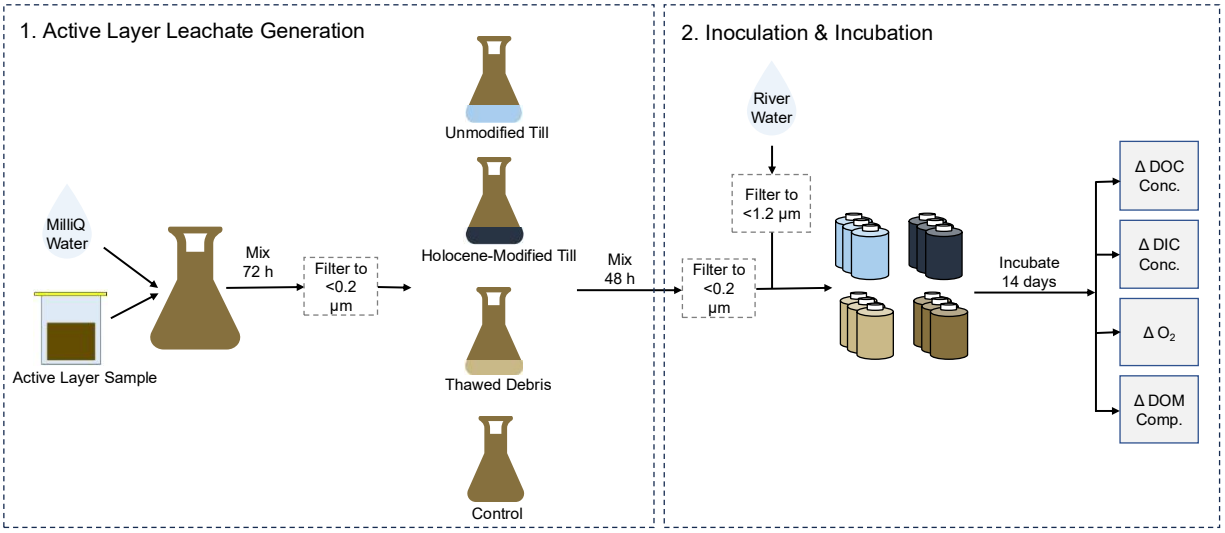

Figure S2. Schematic diagram illustrating the bio-incubation experiment.

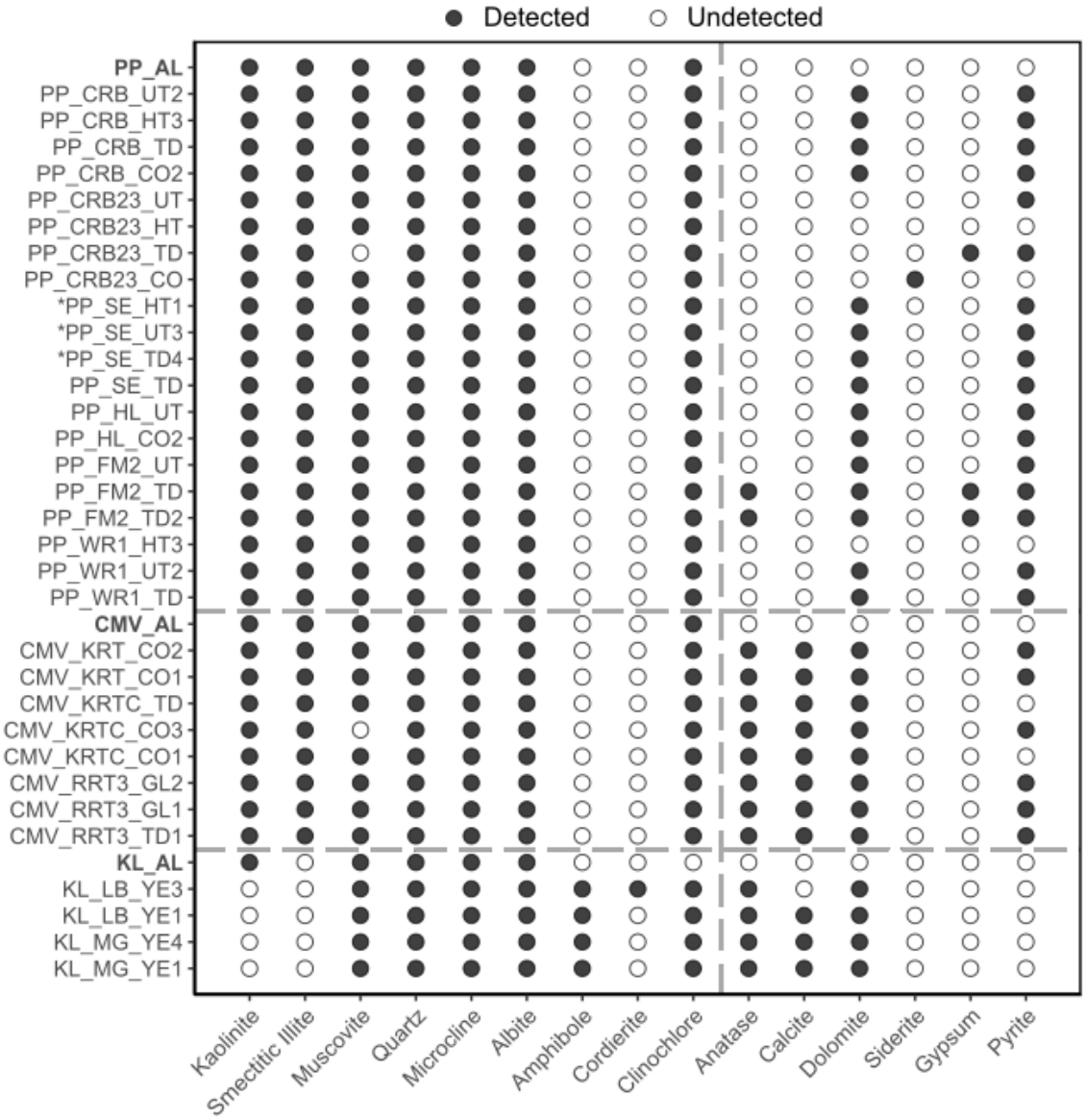

Figure S3. Detection of minerals by X-ray diffraction in sediment samples from northwestern Canada. Horizontal dashed lines divide the three geographic subregions (PP = Peel Plateau, NT; CMV = central Mackenzie Valley, NT; and KL = Klondike, YT). Active layer samples are bolded, and samples included in the bio-incubation experiments are indicated with an asterisk. The vertical dashed line separates silicate minerals (left) and non-silicate minerals (right). Minerals are ordered to indicate relative degree of soil development (Cornelis et al., 2011), with the most stable minerals on the left. Site codes follow Table S1; sediment types are abbreviated as AL (active layer), UT (unmodified till), HT (Holocene-modified till), TD (thawed debris), CO (colluvium), GL (glaciolacustrine), and YE (yedoma).

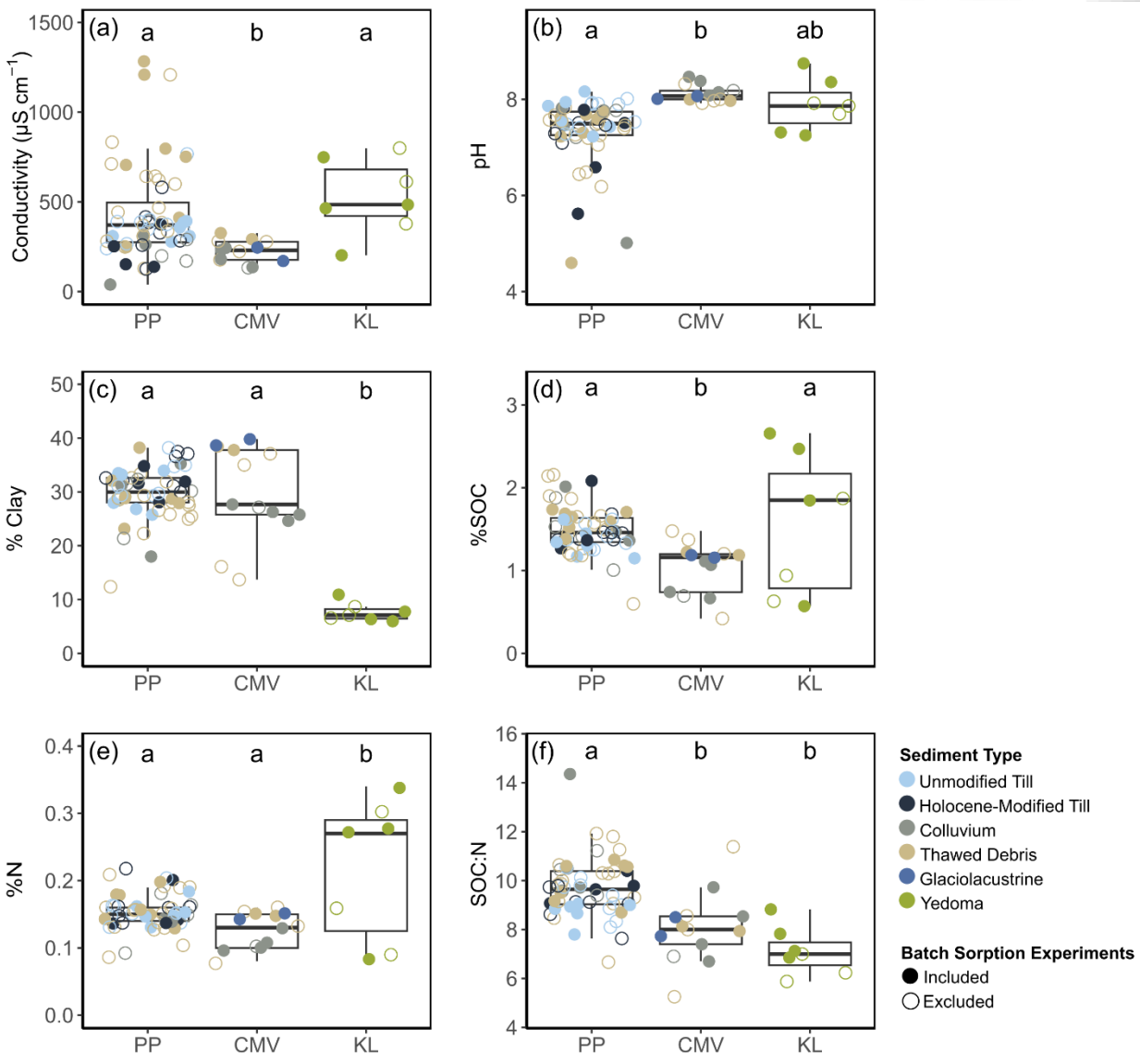

Figure S4. Box and whisker plots of sediment properties of permafrost and debris samples from the Peel Plateau, NT (PP; $n = 56$); central Mackenzie Valley, NT (CMV; $n = 13$); and Klondike region, YT (KL; $n = 7$)). (a) conductivity (µS cm^{-1}), (b) pH, (c) clay content (%), (d) sediment organic carbon content (%), (e) sediment nitrogen content (% SOC), and (f) ratio of sediment organic carbon to total nitrogen (SOC:N). Filled circles represent samples with sorption properties evaluated through batch sorption experiments. Different letters above each region reflect significantly different means (Tukey's HSD, $p < 0.05$).

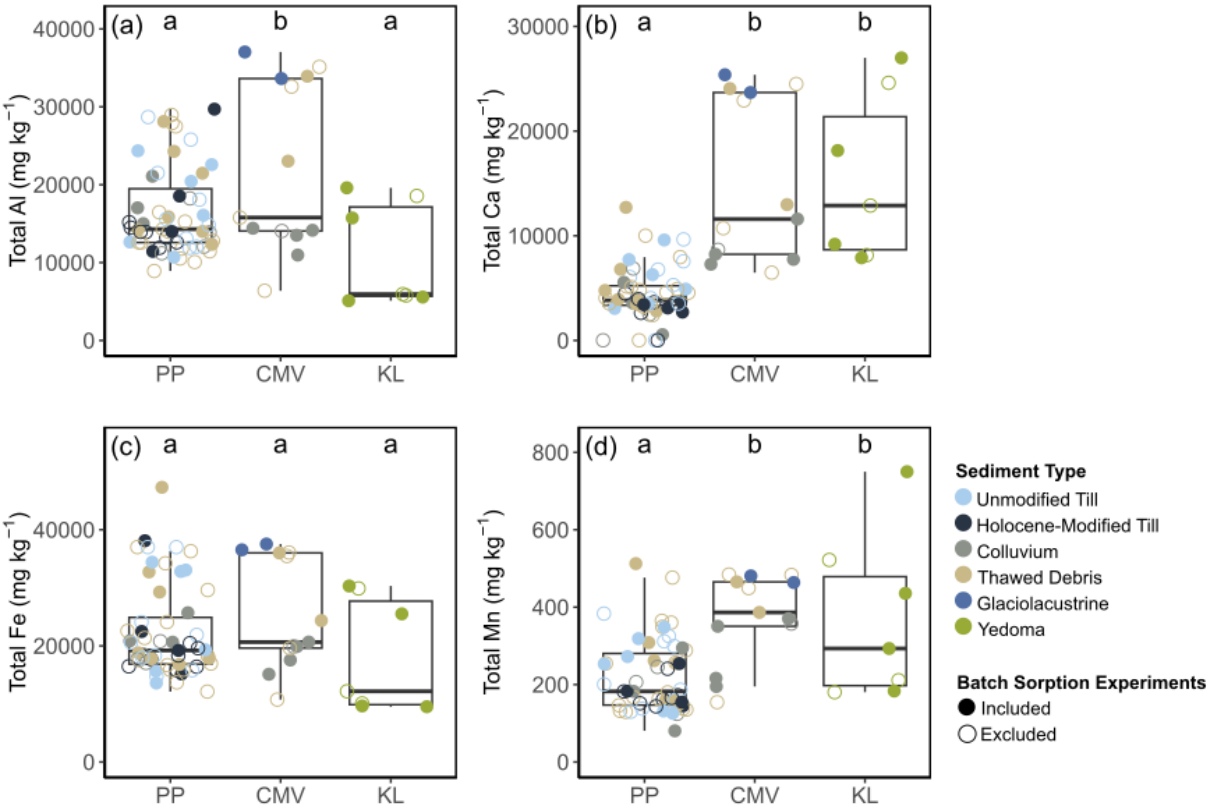

Figure S5. Box and whisker plots of total element concentrations in sediments from the Peel Plateau, NT (PP; *n* = 56); central Mackenzie Valley, NT (CMV; *n* = 13); and Klondike region, YT (KL; *n* = 7)). (a) Al_t, (b) Ca_t, (c) Fe_t, and (d) Mn_t concentrations (mg kg^{-1}). Filled circles represent samples with sorption properties evaluated through batch sorption experiments. Different letters above each region reflect significantly different means (Tukey's HSD, $p < 0.05$).

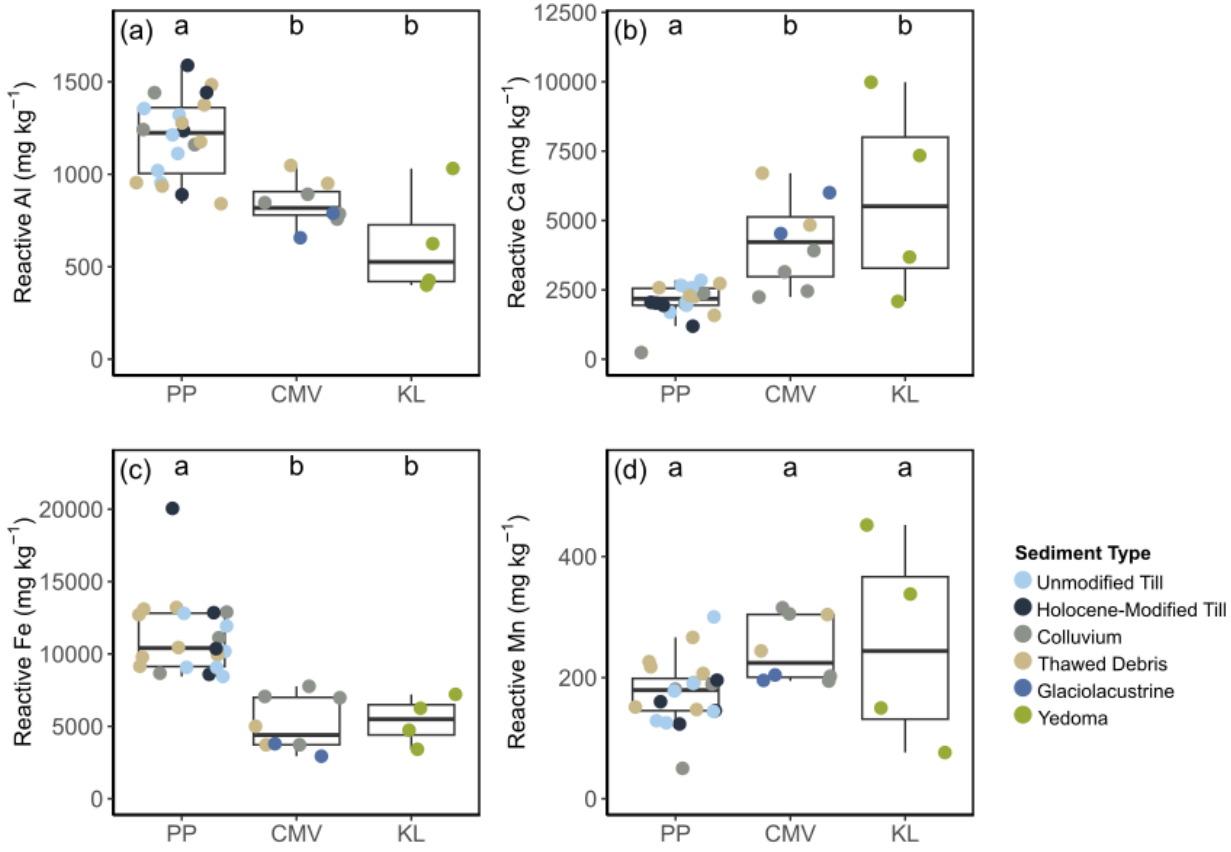

Figure S6. Box and whisker plots of reactive element concentrations in sediments from the Peel Plateau, NT (PP; *n* = 20); central Mackenzie Valley, NT (CMV; *n* = 8); and Klondike region, YT (KL; *n* = 4)). A dark ammonium oxalate extraction was used to determine reactive (a) Al, (c) Fe, and (d) Mn concentrations (mg kg^{-1}); a pyrophosphate extraction was used to determine reactive (b) Ca (mg kg^{-1}). Different letters above each region reflect significantly different means (Tukey's HSD, $p < 0.05$).

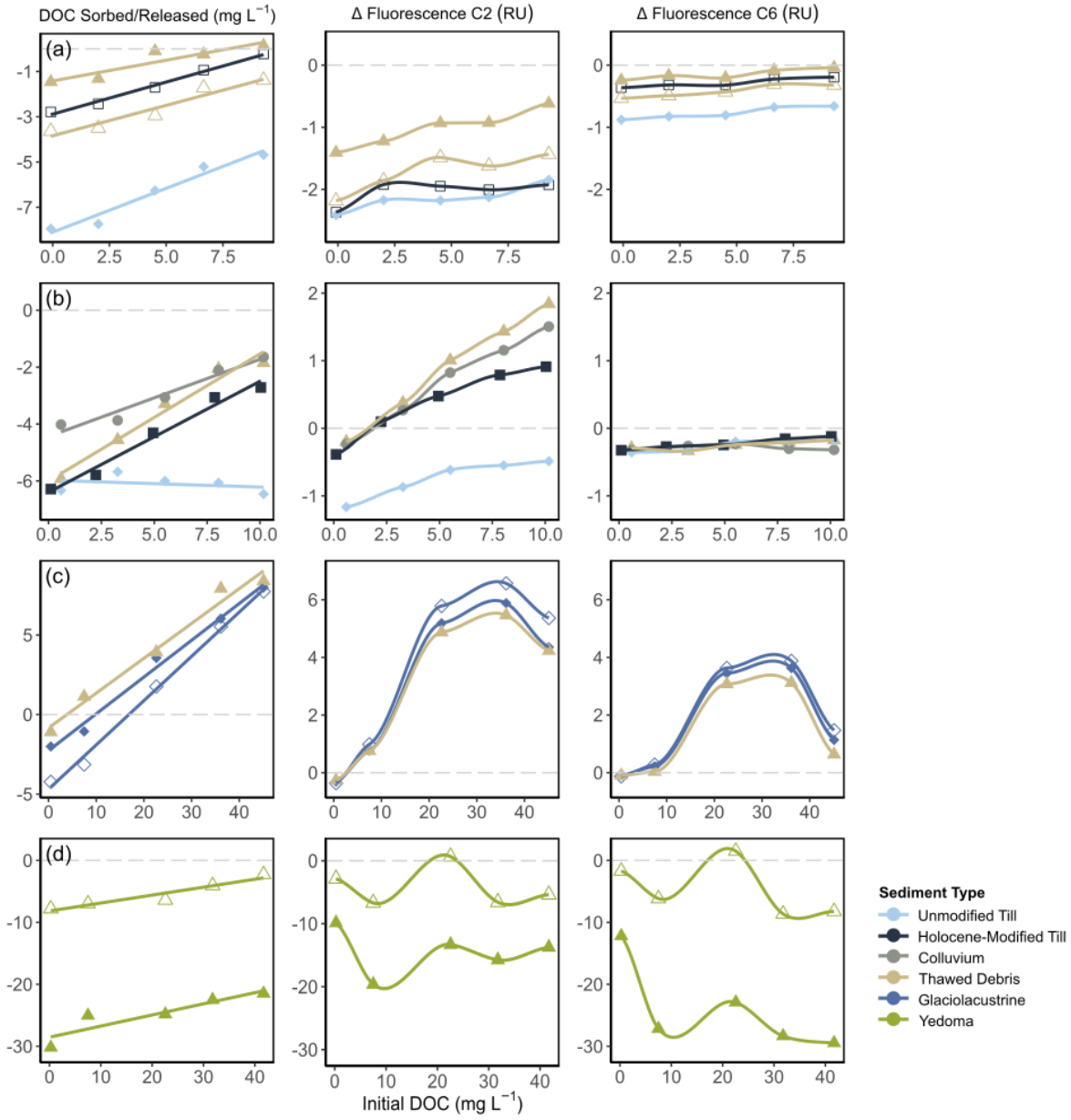

Figure S7. Relationships between initial dissolved organic carbon (DOC; mg L^{-1}) concentration and sorption of different pools of DOC after exposure to sediments. Sorption of total DOC, aromatic (C2; Raman units (RU)) DOM, and protein-like (C6; RU) DOM are shown for sediments from four sites in northwestern Canada: (a) SE on the Peel Plateau, NT; (b) CRB23 on the Peel Plateau, NT; (c) RRT3 in the central Mackenzie Valley, NT; and (d) MG from the Klondike region, YT. Colours represent sediment type and shape fills are used to distinguish multiple samples of the same sediment type from one site. Note that the range of initial DOC values varies between sites.

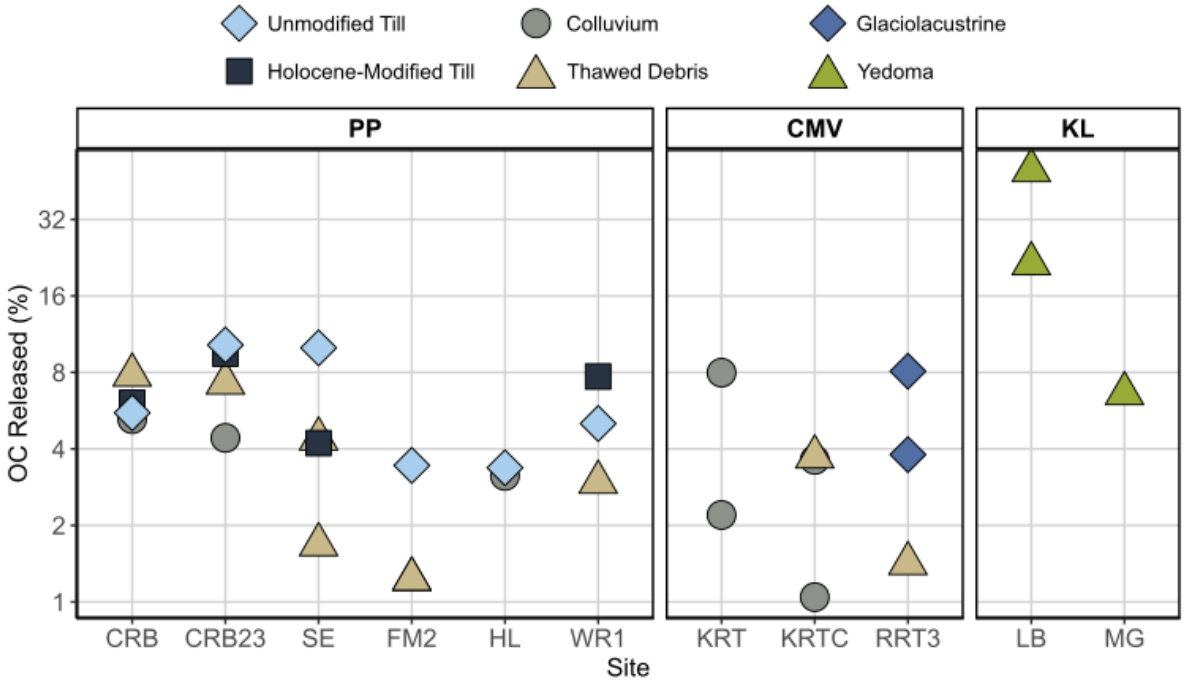

Figure S8. Point plots of the percentage (%) of organic carbon released from permafrost sediments, as water-extractable DOC:SOC. Samples of different sediment types were collected from different sites across three geographic regions (Peel Plateau, NT (PP); central Mackenzie Valley, NT (CMV); Klondike region, YT (KL)). Note that the y-axis is shown in log scale.

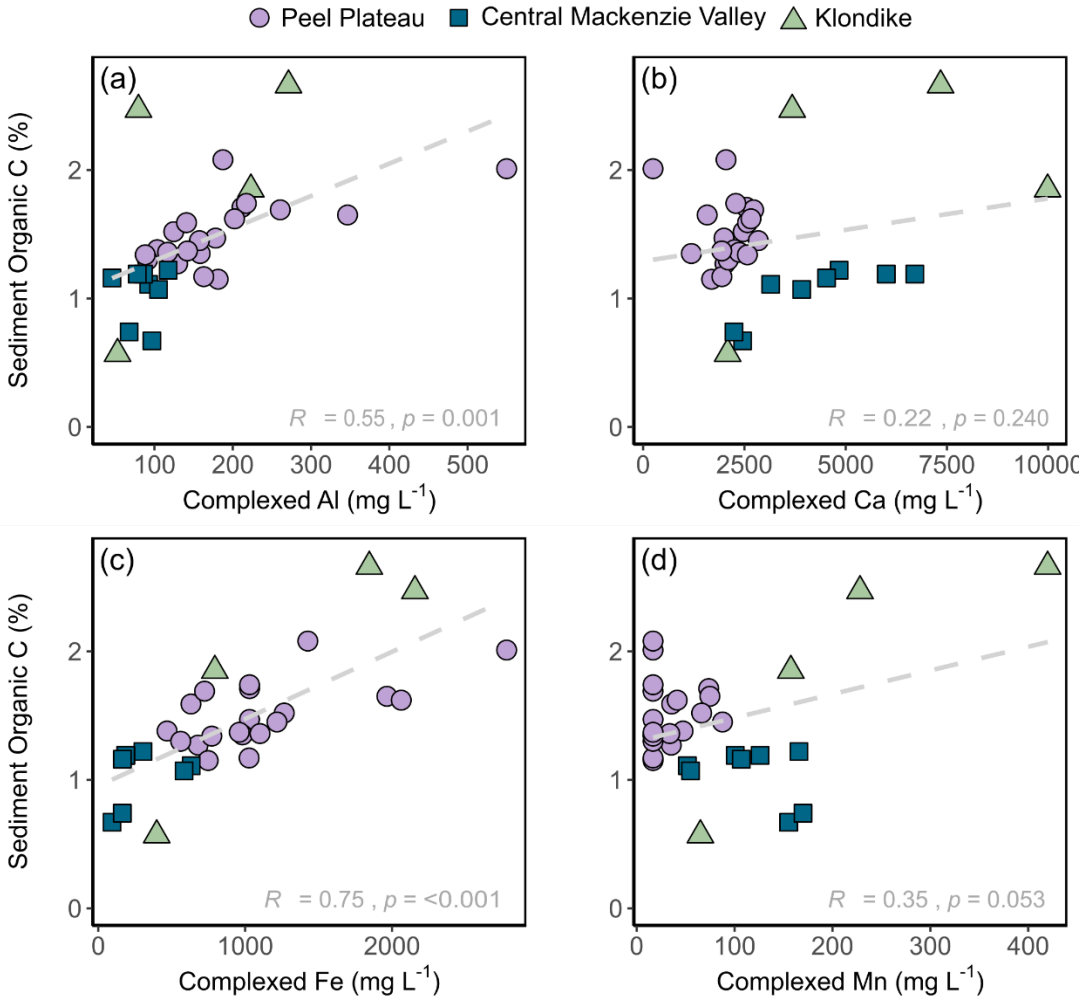

Figure S9. Scatter plots of relationships between sediment organic carbon content (%SOC) and the concentration of elements (mg kg^{-1}) extracted by pyrophosphate (organo-complexed; (a) Al, (b) Ca, (c) Fe, and (d) Mn). Simple linear regressions are represented by a dashed grey line with *R* and *p* values reported at the bottom of each panel.

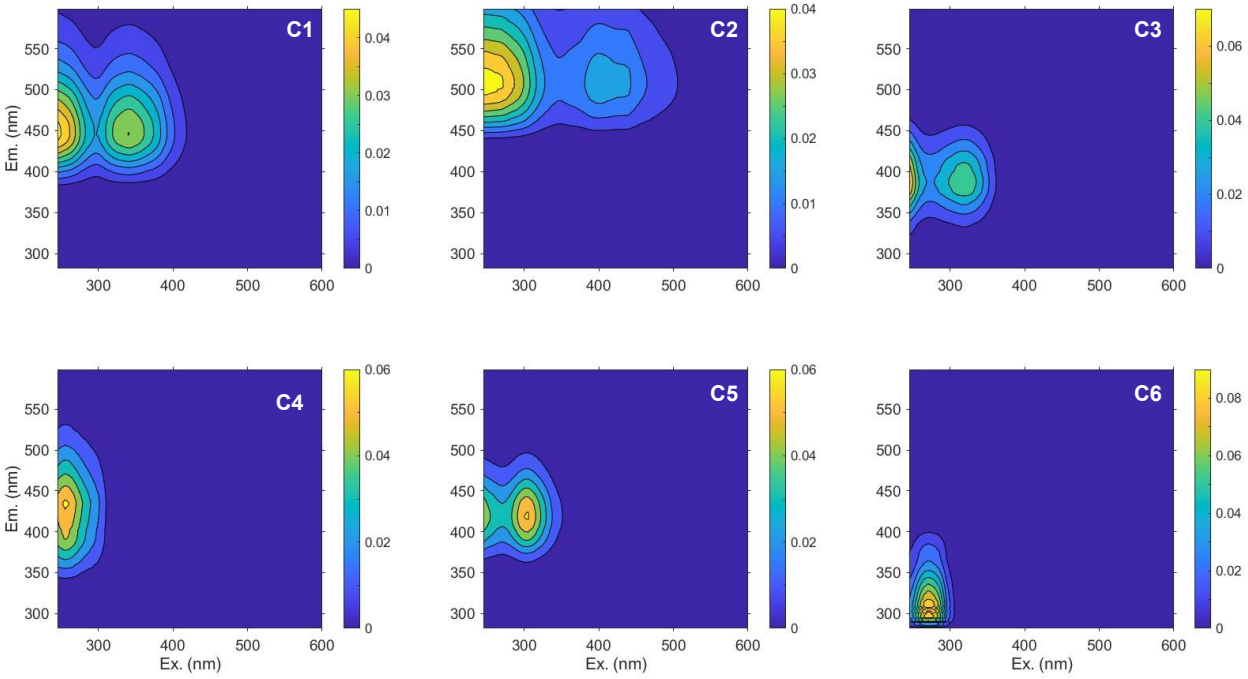

Figure S10. Excitation-Emission matrices of Parallel Factor (PARAFAC) analysis components. PARAFAC components were derived from dissolved organic matter (DOM) samples from solutions from batch sorption (n = 374) experiment and incubation (n = 37; n_{total} = 411). Colour represents fluorescence intensity in Raman units.

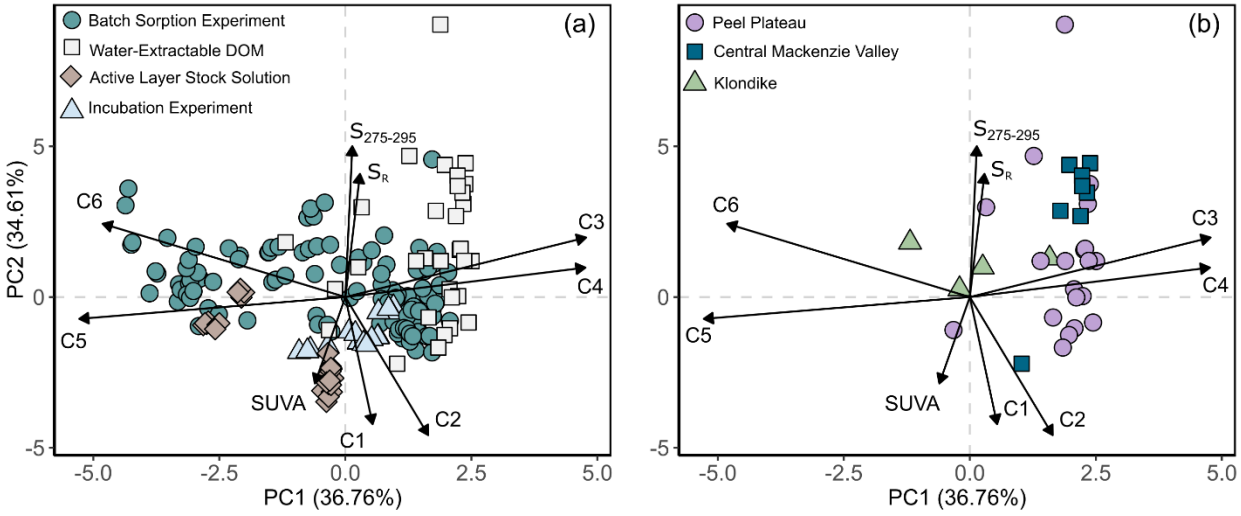

Figure S11. Principal Component Analysis (PCA) plots of dissolved organic matter (DOM) properties. (a) PCA of DOM properties of stock solutions extracted from active layer sediments (n = 32), water-extractable DOM (n = 32), solutions following batch sorption experiments (n = 128), and solutions following incubation experiments (n = 16; n_{total} = 208). Compositional indices are as follows: $S_{275-295}$ – Slope of absorbance 275-295 nm, S_R – Slope Ratio, SUVA – Specific Ultraviolet Absorbance at 254nm, C1-6 – PARAFAC Components 1-6 (see Table S4). (b) PCA of DOM properties (same global PCA as (a)) showing DOM extracted from sediments in a carbon-free solution (water-extractable DOM) by region.

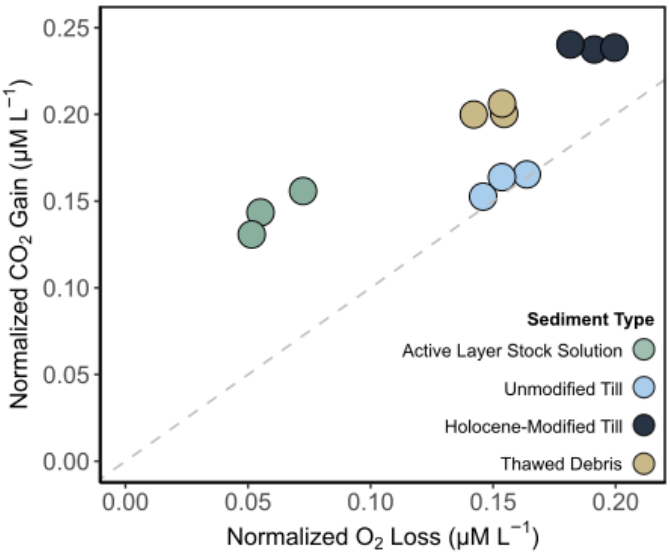

Figure S12. Carbon mineralization metrics from incubation experiments of organic solutions exposed to thawed permafrost sediments. Biplot shows increase in CO_2 (µM L^{-1}) compared to decrease in O_2 (µM L^{-1}) from the start to the end of the incubation experiment, normalized to the initial total organic carbon of the solution. The dashed grey line represents 1:1 molar ratio of CO_2:O_2.

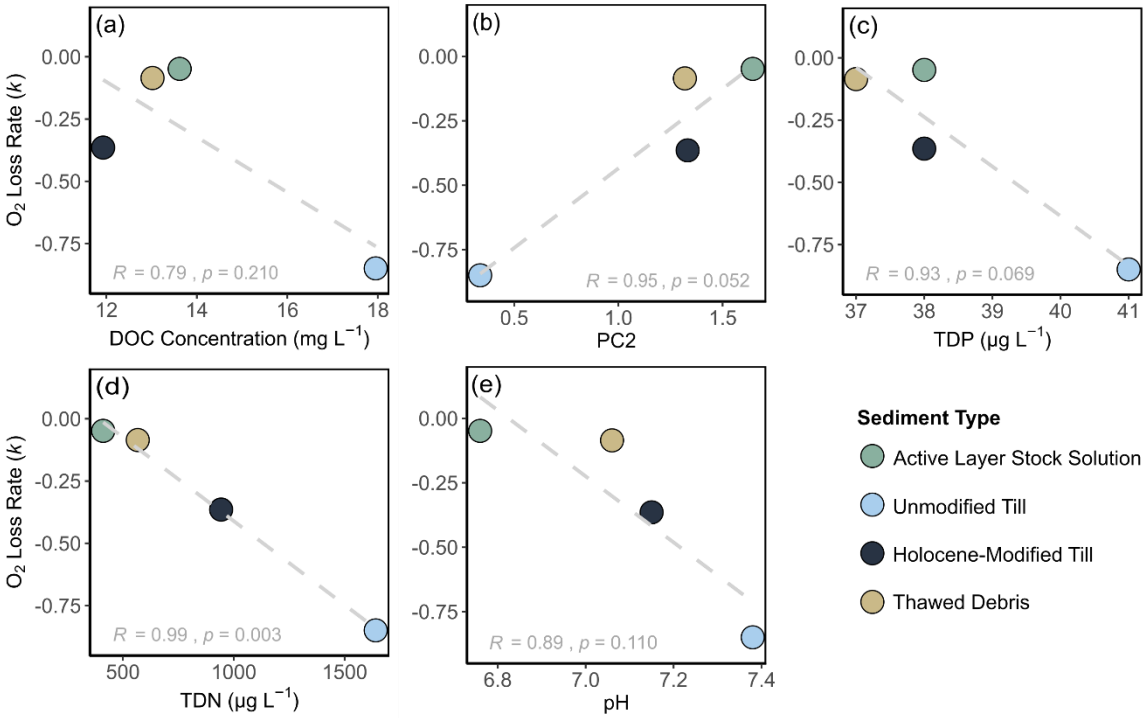

Figure S13. Oxygen loss rates throughout incubations related to initial biogeochemical properties of organic solutions exposed to thawed permafrost sediments. (a) dissolved organic carbon concentration (mg L^{-1}), (b) principal component 2 (PC2; Fig. S8) representing a gradient -from aliphatic, low molecular weight (least negative scores) to aromatic, high molecular weight compounds (most negative scores), (c) total dissolved phosphorous (TDP) concentration (µg L^{-1}), (d) total dissolved nitrogen (TDN) concentration (µg L^{-1}), and (e) pH. Simple linear regressions are represented by a dashed grey line with *R* and *p* values reported in each panel.

References

Chen, S., Du, Y., Das, P., Lamore, A. F., Dimova, N. T., Elliott, M., Broadbent, E. N., Roebuck., J. A., Jaffé, R., and Lu, Y.: Agricultural land use changes stream dissolved organic matter via altering soil inputs to streams, Sci. Total Environ., 796, 148968, https://doi.org/10.1016/j.scitotenv.2021.148968, 2021.

Coble, P. G.: Characterization of marine and terrestrial DOM in seawater using excitation-emission matrix spectroscopy, Mar. Chem., 51, 325–346, https://doi.org/10.1016/0304-4203(95)00062-3, 1996.

Cornelis, J.-T., Delvaux, B., Georg, R. B., Lucas, Y., Ranger, J., and Opfergelt, S.: Tracing the origin of dissolved silicon transferred from various soil-plant systems towards rivers: a review, Biogeosciences, 8, 89–112, https://doi.org/10.5194/bg-8-89-2011, 2011.

Cory, R. M. and McKnight, D. M.: Fluorescence spectroscopy reveals ubiquitous presence of oxidized and reduced quinones in dissolved organic matter, Environ. Sci. Technol., 39, 8142–8149, https://doi.org/10.1021/es0506962, 2005.

Dainard, P. G., Guéguen, C., McDonald, N., and Williams, W. J.: Photobleaching of fluorescent dissolved organic matter in Beaufort Sea and North Atlantic Subtropical Gyre, Mar. Chem., 177, 630–637, https://doi.org/10.1016/j.marchem.2015.10.004, 2015.

DeFrancesco, C. and Guéguen, C.: Long-term trends in dissolved organic matter composition and its relation to sea ice in the Canada Basin, Arctic Ocean (2007–2017), J. Geophys. Res.-Oceans, 126, e2020JC016578, https://doi.org/10.1029/2020JC016578, 2021.

Kaiser, K., Guggenberger, G., and Zech, W.: Sorption of DOM and DOM fractions to forest soils, Geoderma, 74, 281–303, https://doi.org/10.1016/S0016-7061(96)00071-7, 1996.

Kokelj, S. V., Lacelle, D., Lantz, T. C., Tunnicliffe, J., Malone, L., Clark, I. D., and Chin, K. S.: Thawing of massive ground ice in mega slumps drives increases in stream sediment and solute flux across a range of watershed scales, J. Geophys. Res.-Earth, 118, 681–692, https://doi.org/10.1002/jgrf.20063, 2013.

Kothawala, D. N., Stedmon, C. A., Müller, R. A., Weyhenmeyer, G. A., Köhler, S. J., and Tranvik, L. J.: Controls of dissolved organic matter quality: evidence from a large-scale boreal lake survey, Global Change Biol., 20, 1101–1114, https://doi.org/10.1111/gcb.12488, 2014.

Lambert, T., Bouillon, S., Darchambeau, F., Massicotte, P., and Borges, A. V.: Shift in the chemical composition of dissolved organic matter in the CongoRiver network, Biogeosciences, 13, 5405–5420, https://doi.org/10.5194/bg-13-5405-2016, 2016.

Littlefair, C. A. and Tank, S. E.: Biodegradability of thermokarst carbon in a till-associated, glacial margin landscape: The case of the Peel Plateau, NWT, Canada, J. Geophys. Res.-Biogeosci., 123, 3293–3307, https://doi.org/10.1029/2018JG004461, 2018.

Malone, L., Lacelle, D., Kokelj, S., and Clark, I. D.: Impacts of hillslope thaw slumps on the geochemistry of permafrost catchments (Stony Creek watershed, NWT, Canada), Chem. Geol., 356, 38–49, https://doi.org/10.1016/j.chemgeo.2013.07.010, 2013.

Mopper, K. and Kieber, D. J.: Marine photochemistry and its impact on carbon cycling, in: The Effects of UV Radiation in the Marine Environment, edited by: De Mora, S., Demers, S., and Vernet, M., Cambridge University Press, 101–129, https://doi.org/10.1017/CBO9780511535444.005, 2000.

Orlova, J., Amiri, F., Bourgeois, A. K., Buttle, J. M., Cherlet, E., Cuss, C. W., Devito, K. J., Emelko, M. B., Floyd, W. C., Foster, D. E., Hutchins, R. H. S., Jamieson, R., Johnson, M. S., McSorley, H. J., Silins, U., Tank, S. E., Thompson, L. M., Webster, K. L., Williams, C. H. S., and Olefeldt, D.: Composition of stream dissolved organic matter across Canadian forested ecozones varies in three dimensions linked to landscape and climate, Water Resour. Res., 60, e2023WR035196, https://doi.org/10.1029/2023WR035196, 2024.

Osburn, C. L., Anderson, N. J., Stedmon, C. A., Giles, M. E., Whiteford, E. J., McGenity, T. J., Dumbrell, A. J., and Underwood, G. J. C.: Shifts in the source and composition of dissolved organic matter in southwest Greenland lakes along a regional hydro-climatic gradient, J. Geophys. Res.-Biogeosci., 122, 3431–3445, https://doi.org/10.1002/2017JG003999, 2017.

Podgorski, D. C., Zito, P., McGuire, J. T., Martinovic-Weigelt, D., Cozzarelli, I. M., Bekins, B. A., and Spencer, R. G. M.: Examining natural attenuation and acute toxicity of petroleum-derived dissolved organic matter with optical spectroscopy, Environ. Sci. Technol., 52, 6157–6166, https://doi.org/10.1021/acs.est.8b00016, 2018.

R Core Team: R: A language environment for statistical computing, 2024.

Walker, S. A., Amon, R. M. W., Stedmon, C., Duan, S., and Louchouarn, P.: The use of PARAFAC modeling to trace terrestrial dissolved organic matter and fingerprint water masses in coastal Canadian Arctic surface waters, J. Geophys. Res.-Biogeosci., 114, 2009JG000990, https://doi.org/10.1029/2009JG000990, 2009.

Wickham, H.: ggplot2: Elegant graphics for data analysis, 2016.

Wickham, H., Averick, M., Bryan, J., Chang, W., McGowan, L., François, R., Grolemund, G., Hayes, A., Henry, L., Hester, J., Kuhn, M., Pedersen, T., Miller, E., Bache, S., Müller, K., Ooms, J., Robinson, D., Seidel, D., Spinu, V., Takahashi, K., Vaughan, D., Wilke, C., Woo, K., and Yutani, H.: Welcome to the Tidyverse, JOSS, 4, 1686, https://doi.org/10.21105/joss.01686, 2019.

Wickham, H., François, R., Henry, L., Müller, K., and Vaughan, D.: dplyr: A grammar of data manipulation, 2023.

Zolkos, S., Tank, S. E., Striegl, R. G., and Kokelj, S. V.: Thermokarst effects on carbon dioxide and methane fluxes in streams on the Peel Plateau (NWT, Canada), J. Geophys. Res.-Biogeosci., 124, 1781–1798, https://doi.org/10.1029/2019JG005038, 2019.

Zolkos, S., Tank, S. E., Kokelj, S. V., Striegl, R. G., Shakil, S., Voigt, C., Sonnentag, O., Quinton, W. L., Schuur, E. A. G., Zona, D., Lafleur, P. M., Sullivan, R. C., Ueyama, M., Billesbach, D., Cook, D., Humphreys, E. R., and

Marsh, P.: Permafrost landscape history shapes fluvial chemistry, ecosystem carbon balance, and potential
250 trajectories of future change, Global Biogeochem. Cy., 36, https://doi.org/10.1029/2022GB007403, 2022.